Superlattice-doped silicon detectors: progress and prospects

Michael E. Hoenk*[a], Shouleh Nikzad[a], Alexander G. Carver[a], Todd J. Jones[a], John Hennessy[a], April D. Jewell[a], Joseph Sgro,[b], Shraga Tsur[c], Mickel McClish[d], Richard Farrell[d]
[a]Jet Propulsion Laboratory, California Institute of Technology, 4800 Oak Grove Dr., Pasadena, CA, USA 91109; [b]Alacron Inc., 71 Spit Brook Rd., Suite 200, Nashua, NH 03060;
[c]Applied Materials Inc., Process, Diagnostics & Control, 9 Oppenheimer St., Rehovot, Israel, 76075;
[d]Radiation Monitoring Devices, Inc., 44 Hunt Street, Watertown, MA, USA 02472

ABSTRACT

In this paper we review the physics and performance of silicon detectors passivated with wafer-scale molecular beam epitaxy (MBE) and atomic layer deposition (ALD). MBE growth of a two-dimensional (2D) doping superlattice on backside-illuminated (BSI) detectors provides nearly perfect protection from interface traps, even at trap densities in excess of 10^{14} cm^{-2}. Superlattice-doped, BSI CMOS imaging detectors show no measurable degradation of quantum efficiency or dark current from long-term exposure to pulsed DUV lasers. Wafer-scale superlattice-doping has been used to passivate CMOS and CCD imaging arrays, fully-depleted CCDs and photodiodes, and large-area avalanche photodiodes. Superlattice-doped CCDs with ALD-grown antireflection coatings achieved world record quantum efficiency at deep and far ultraviolet wavelengths (100-300nm). Recently we have demonstrated solar-blind, superlattice doped avalanche photodiodes using integrated metal-dielectric coatings to achieve selective detection of ultraviolet light in the 200-250 nm spectral range with high out-of-band rejection.

Keywords: Superlattice doping, silicon detectors, MBE, ALD, CCD, CMOS, APD, back illumination

1. INTRODUCTION

1.1 Challenge and paradox: Atomic scale control over surfaces and interfaces

The challenge and paradox of ultraviolet detectors is that detection and damage are inseparable at high photon energies. Molecular beam epitaxy (MBE) and atomic layer deposition (ALD) provide a way out of this paradox. By engineering surfaces and interfaces with atomic-scale precision, we can achieve exceptional quantum efficiency and stability against UV-induced surface damage.

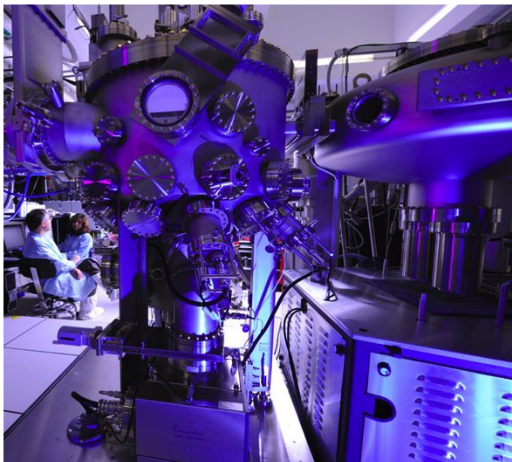

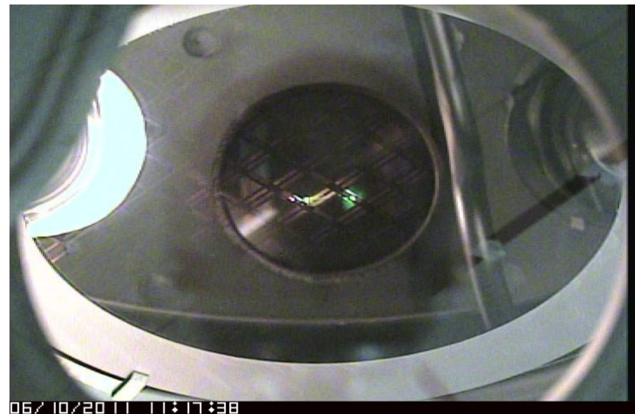

Figure 1: JPL's Gen200 MBE system enables production-scale passivation of backside-illuminated detectors. The photograph on the left shows the growth chamber and cluster tool for automated wafer transfer and growth. The photograph on the right shows a 200 mm detector wafer during MBE growth of a 2D doping superlattice.

* Michael.E.Hoenk@jpl.nasa.gov; phone 1-818-354-1881; fax 1-818-393-3302; microdevices.jpl.nasa.gov

High Energy, Optical, and Infrared Detectors for Astronomy VI, edited by Andrew D. Holland, James Beletic, Proc. of SPIE Vol. 9154, 915413 · © 2014 SPIE · CCC code: 0277-786X/14/$18 · doi: 10.1117/12.2057678

Downloaded From: http://spiedigitallibrary.org/ on 02/05/2015 Terms of Use: http://spiedl.org/terms

Since JPL's invention of MBE as a tool for surface passivation of backside illuminated (BSI) imaging arrays, delta-doped detectors have demonstrated nearly 100% internal quantum efficiency (QE) with exceptional stability in back-illuminated CCD, CMOS, PIN diode arrays, and hybrid devices spanning a variety of formats and designs.[1-4] Using ALD, we have further demonstrated world record QE at deep and far ultraviolet wavelengths.[5-7] With the recent acquisition and commissioning of a production-scale silicon MBE system, JPL has greatly expanded its capabilities for producing high-performance delta-doped, back-illuminated imaging arrays with high throughput and high yield (Figure 1).[4,8] Using this system, we demonstrated superlattice-doped CMOS imaging arrays with unprecedented stability under direct illumination with pulsed deep ultraviolet (DUV) lasers.[9-11] Recently we demonstrated superlattice-doped avalanche photodiodes with integrated, solar-blind metal-dielectric coatings, which show excellent promise for scientific and commercial applications.[12,13] Many of these applications require advanced capabilities for photon counting and solar-blind detection. In this paper, we review the latest results of our work on surface passivation and antireflection coatings for BSI detectors using wafer-scale MBE and ALD.

1.2 Surface passivation vs. surface damage: Lessons from the SOHO Extreme Ultraviolet Instrument

Despite extensive efforts spanning more than 40 years of development, BSI detectors have not achieved sufficient DUV stability for many scientific and commercial applications.[14-16] Whereas BSI silicon detectors perform extremely well at visible and near infrared wavelengths, exposure to deep and far ultraviolet radiation causes surface damage and instabilities. The Extreme Ultraviolet Instrument on SOHO provides a dramatic illustration of the severity of UV-induced surface damage and the limits of conventional surface passivation methods. These CCDs had been passivated using the best available ion implantation and laser anneal processes optimized for high EUV quantum efficiency. Solar EUV radiation caused the loss of over 80% of EUV responsivity, and also led to instabilities that severely compromised photometric accuracy (see Figure 2).[17,18] An investigation of the damage mechanisms revealed that most of the degradation was caused by EUV-induced surface damage, which formed trap states and led to local charging of the native oxide on the exposed detector surface. The surface damage could only be partially annealed, and the resulting instabilities could not be adequately corrected, prompting the European Space Agency to fly a duplicate instrument on a sounding rocket for recalibration and diagnosis. The image and line scans in Figure 2 were collected from the sounding rocket experiment.

Many scientific and commercial applications require detectors to remain stable to better than 1%. This demand has proven very difficult to achieve. The fundamental problem is that none of the conventional passivation methods are stable against high densities of interface traps. Even with the best available methods for oxidation and passivation, interface trap densities in the range of 10^{14} $cm^{-2}eV^{-1}$ have been measured after exposure to vacuum ultraviolet radiation.[19] The unsolved challenge of passivation lies in stabilizing devices even at this level of damage. Extensive efforts have been made to suppress the damage by developing radiation-hardened oxides.[15,20-23] Methods for doing this include improving oxidation processes to reduce the water content and defect density, thinning oxides to reduce the cross section for damage, and developing multilayer oxides using materials such as silicon nitride that are more radiation-hard than SiO_2. Nitrided oxides developed for front-illuminated silicon photodiodes are formed at high temperatures (1065°C), which is not compatible with BSI detectors.[21-22] BSI detectors that remain stable against damage from deep and far ultraviolet radiation have remained elusive.[14-16] JPL's passivation methods enable BSI detectors with unique stability and QE by using low-temperature MBE and ALD processes for atomic-scale engineering of the silicon surface.[9-11]

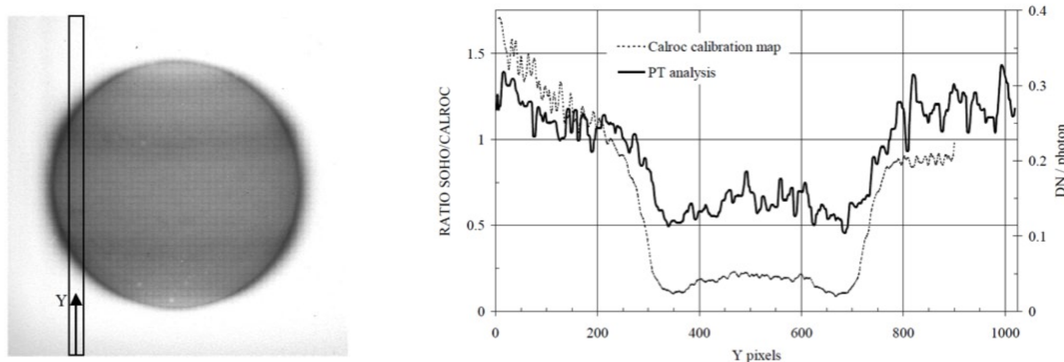

Figure 2. Comparison of back-illuminated, ion-implanted CCD response before and after exposure to solar extreme ultraviolet radiation demonstrates severe, permanent damage caused by traps formed at the Si-SiO_2 interface.

Downloaded From: http://spiedigitallibrary.org/ on 02/05/2015 Terms of Use: http://spiedl.org/terms

2. SURFACE PASSIVATION OF SILICON DETECTORS

2.1 Surface passivation of BSI detectors

The surface of thinned, BSI detectors is comprised of high purity silicon, which is extremely sensitive to charge in oxides and interfaces. At thermal equilibrium, charge transfer from silicon to interface traps "pins" the surface Fermi level in the middle of the bandgap. In p-type silicon surfaces, interface traps acquire a net positive charge. Defects and contaminants create a fixed density of charge in the oxide, while interface traps capture majority carriers at the Si-SiO_2 interface. The physical location of traps in the oxide plays an important role in the dynamics of the illuminated surface. Interface traps are located within ~1 nm of the silicon surface, which puts them within tunneling distance of the silicon. Interface traps are therefore capable of changing charge state in response to transient changes in the surface potential. Traps located deeper in the oxide change state much more slowly.

As illustrated by SOHO CCDs, interface traps destabilize detectors through dynamic interactions with photogenerated charge. Illumination drives the surface away from equilibrium, causing the back surface potential to vary over the width of the bandgap. Ultraviolet detectors are especially sensitive to variations in surface charge, because the absorption length of UV photons is less than 10 nm over nearly the entire spectral range from 100-400 nm. As a result, unpassivated BSI detectors are subject to extreme variations in QE and dark current, which are manifest as hysteresis and persistence in the detector response. Exposure to ultraviolet light and other forms of ionizing radiation enhances these variations by damaging surfaces. Because these instabilities are caused by an electrically active surface, methods to mitigate these effects are referred to as surface passivation. Surface passivation mitigates the effects of variable surface charge on detector performance, but cannot eliminate them entirely.

Since the first BSI CCDs were demonstrated in 1973, many methods have been developed for back surface passivation. These can be roughly divided into backside charging and back surface doping technologies, which are distinguished by the location and distribution of charge in the detector and its oxide. Backside charging methods stabilize the detector by introducing negative charge into the oxide. Provided that the density of interface traps is not too high, the negatively charged passivation layer will bias the surface into accumulation (see Section 2.2). Backside doping methods take the opposite approach, by introducing an impurity profile that stabilizes the surface and creates an internal bias in the detector (see Section 2.3).

2.2 Field-induced passivation

In order to achieve and maintain high, stable QE, BSI detectors require a strong electric field near the surface. The electric field drives photogenerated electrons away from the back surface and toward the front-surface collection wells. Field-induced passivation methods, also known as backside charging, seek to overcome variations in interface charge density by forming a surface passivation layer with a stable, negative charge. The negative charge density must be sufficient to bias the surface into accumulation in order to create a near surface electric field and form a conductive surface. Among the various approaches that have been used for BSI detectors are the UV flood, platinum flash gate, biased flash gate, and chemisorption charging.[23-25]

Field-induced exclusion of minority carriers from the surface suppresses surface recombination and dark current generation processes that are responsible for inefficiency and noise. Because both surface and bulk processes influence recombination rates, the magnitude and direction of the near-surface electric field are critical to the exclusion of minority carriers from the surface and the attainment of high charge collection efficiency.

Early work in the field showed that the electric field near the surface should be at least 2 to 3×10^4 V/cm in order to keep photogenerated charge from reaching the surface.[24-26] Given that fixed oxide charge densities on the order of 10^{12} cm^{-2} have been measured in high quality oxides used for backside charging, the minimum density of negative charge required for BSI detector passivation is in the high 10^{12} cm^{-2} range.[23] Charge densities in this range produce an electric field on the order of 10^5 V/cm in the critical near-surface region of the silicon detector.

Provided that the interface trap density remains sufficiently low, backside charging enables detectors to achieve the highest possible QE in the visible and near ultraviolet spectral range. There are two reasons for this. First, the electric field produced by surface charging extends all the way to the semiconductor surface, providing effective field-induced passivation of interface traps and suppression of back surface recombination.[24] Second, the oxide required to stabilize the back surface charge also functions as an antireflection coating.

Despite these advantages, backside charging is not the preferred method of passivation for spaceflight for several reasons.[26] First, because the surface is comprised of high purity silicon, the near-surface electric field is especially

Downloaded From: http://spiedigitallibrary.org/ on 02/05/2015 Terms of Use: http://spiedl.org/terms

sensitive to environmentally-induced variability in oxide and interface charge. Second, the detection of high-energy photons (e.g., far and extreme ultraviolet) is compromised by absorption and degradation of the thick oxides required for stable backside charging. Third, some methods of backside charging are vulnerable to environmental conditions, thus requiring packaging in a controlled environment. Finally, damage can be severe enough to reverse the polarity of the surface charge, in which case passivation fails completely.

2.3 Surface doping and the surface depletion layer

Whereas field-induced passivation biases the surface into accumulation, highly doped surfaces are typically depleted by charge trapped in interface states. Highly doped surfaces are subject to trapping and recombination of photogenerated charge in the depletion layer, and also to higher bulk recombination rates. Surface doping is therefore more susceptible to surface recombination than field-induced passivation.[24-26] The disadvantages of backside charging were discussed in Section 2.2. The advantage of surface doping lies in the potentially greater stability that can be achieved. In particular, surface doping promises greater resistance to radiation-induced traps.

In p-type surfaces, holes are trapped in interface states. This charge transfer depletes the surface of holes, forming a depletion layer with a negative net charge density. The surface is therefore characterized by a charge dipole, bounded on one side by positive charge in the surface/oxide and on the other by the negatively charged depletion layer. To a first approximation, the depth of the depletion layer is given by the ratio of surface charge density to silicon dopant density. Thus, variations in the surface charge density are reflected by variations in the depletion layer depth. Within the depletion layer, photogenerated electrons experience a force directed toward the surface where they can be lost to trapping and recombination.

Back surface doping methods seek to create a near-surface doping profile that simultaneously shrinks the surface depletion layer and creates a strong, built-in electric field. Controlling the doping profile can stabilize the detector against variations in surface charge density. Ideally, surface doping achieves a high near-surface dopant concentration with a strong gradient, thereby creating a surface that is insensitive to charge trapped at the surface. Surface doping is potentially more stable than back surface charging in challenging environments, including in particular high radiation environments in space.

2.4 Ion implantation and annealing

Ion implantation is currently the most common passivation method used for scientific detectors in space instruments.[26,27] This method is based on directing a beam of dopant atoms (or molecular precursors, such as BF_2) toward the surface with energies on the order of several keV. The range and profile shape depend on the beam energy; for detectors, shallow profiles are preferred, which requires low energy implantation. Ion implantation damages the silicon lattice, and most dopant atoms end up in interstitial sites, where they act as defects rather than dopants. A high temperature annealing process is therefore required to recrystallize damaged silicon and electrically activate dopants. This is usually done with lasers in order to avoid thermally damaging the detector electronics. Even with laser annealing, the temperature is high enough to cause a redistribution of dopants, altering the near-surface doping gradient. Typical peak dopant concentrations used for detectors are in the 10^{18} – 10^{19} cm^{-3} range, with a junction depth of several hundred nanometers. For optimal performance, the surface is sometimes etched after implantation/anneal to increase the near-surface doping gradient.

In practice, ion implantation affords limited control over the critical parameters that affect detector efficiency and stability. The limits of sensitivity and stability of these detectors are determined by the doping profile and trap densities (surface and bulk). Even when used in combination with surface etching, ion implantation typically does not produce a strong enough doping gradient to match the electric field strength achieved by backside charging methods. Furthermore, interface traps induce the formation of a backside potential well that leads to trapping and recombination of photogenerated charge. Thus, ion implantation of BSI detectors requires optimization of multiple processing parameters, and offers limited control over the dopant concentration and depth profile.[25,26] State-of-the-art ion implanted devices are therefore not QE-pinned, prompting the use of back surface charging techniques to stabilize and improve the quantum efficiency.[28,29]

Empirically, ion-implanted BSI detectors achieve optimal quantum efficiency when the surface dopant concentration is in the range of ~10^{18} cm^{-3}. At this doping level, interface trapped charge of ~10^{12} cm^{-2} induces the formation of a surface depletion layer with a thickness of ~10 nm. Because this is comparable to the UV absorption depth in silicon, some loss of signal to recombination is expected. Doping levels in the range of ~10^{19} cm^{-3} reduce the thickness of the surface

Downloaded From: http://spiedigitallibrary.org/ on 02/05/2015 Terms of Use: http://spiedl.org/terms

depletion layer and improve the tolerance to interface traps; however, higher doping also reduces minority carrier lifetime, resulting in lower UV quantum efficiency.

To illustrate these relationships, Figure 3 quantifies the effect of interface traps on ion implanted surfaces. Six-band *k•p* calculations of the surface band structure were applied to simulated ion-implanted surfaces. The models are based on self-consistent solutions of the Poisson and Schrödinger equations.[30] Surface damage is simulated by varying the interface trap density from 10^{12} to 10^{14} $cm^{-2}eV^{-1}$ These calculations illustrate the greater stability that is achieved by increasing the surface dopant concentration. Increasing the peak dopant concentration from $2x10^{18}$ cm^{-3} (2a) to $5x10^{19}$ cm^{-3} (2b), shrinks the surface potential well from 40 nm to 6 nm at the highest trap density, and also increases the electric field strength in the detector bulk from 1 to $5x10^4$ V/cm. Detectors doped to $5x10^{19}$ cm^{-3} can be expected to remain stable at trap densities up to 10^{13} $cm^{-2}eV^{-1}$. However, trap densities approaching 10^{14} $cm^{-2}eV^{-1}$ can cause severe degradation. Note that trap densities exceeding 10^{14} cm^{-2} have been observed in VUV-damaged thermal oxides.[19]

The improved stability achieved by increasing the surface doping concentration must be balanced against the decreased minority carrier lifetime. Ion implantation penetrates to depths of several tenths of a micron from the surface, providing sufficient time for bulk recombination to affect the overall quantum efficiency. In practice, this limitation of ion implantation results in a tradeoff between stability and quantum efficiency.

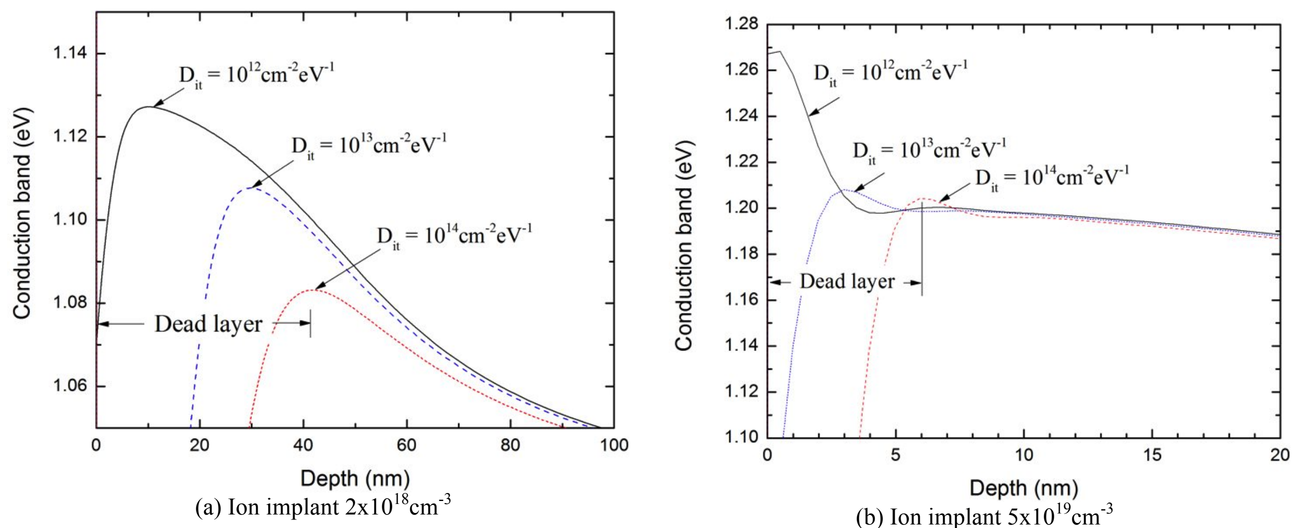

Figure 3. This figure shows the conduction band vs. depth for two ion implanted surfaces. In Figure 3a, the surface dopant concentration is $2x10^{18}$ cm^{-3}, while in Figure 3b it is $5x10^{19}$ cm^{-3}. The effects of surface damage are illustrated by modeling each of these surfaces at three different surface trap densities.

3. STRUCTURE AND PHYSICS OF 2D DOPING SUPERLATTICES

3.1 Growth and structure of two-dimensional (2D) doped silicon

JPL invented low temperature MBE as a method of passivating BSI detectors.[1,31] This approach enables control over the surface doping profile with nearly atomic-scale precision. The first time JPL passivated a CCD using MBE, the passivation layer comprised 5 nm of silicon doped at $3x10^{20}$ cm^{-3}, and a sacrificial 1 nm undoped silicon cap layer to form the surface oxide.[31] In all subsequent devices, JPL has used 2D doping for surface passivation.[1-11] The advantages of 2D-doping over 3D-doping are described in detail below.

The growth of 2D-doped silicon is based on self-organized surface phases that form during sub-monolayer deposition of dopant atoms on silicon. During MBE growth, a thin layer of undoped silicon is grown on the substrate to form an atomically clean, uniform silicon surface. The silicon flux is interrupted by closing a shutter, and boron is deposited on the atomically clean silicon surface, where it spontaneously forms a self-organized surface phase. Once the surface coverage reaches a pre-defined level, the boron shutter is closed and the silicon shutter is opened in order to grow a thin layer of crystalline silicon on the boron-doped surface. This process is termed delta doping, because the resulting vertical dopant profile resembles the mathematical delta function.

Downloaded From: http://spiedigitallibrary.org/ on 02/05/2015 Terms of Use: http://spiedl.org/terms

Unlike conventional "3D" doping methods, in which dopants are randomly distributed in the silicon lattice, 2D doping (also known as delta-doping) incorporates dopant atoms in highly nonrandom, self-organized 2D layers. At concentrations above 3×10^{20} B/cm^3, conventional (3D) suffers from poor quality crystals, in which dopant atoms are only partially activated due to clustering and incorporation into interstitial sites. In contrast, 2D doping is marked by high crystal quality with nearly 100% electrical activation at concentrations exceeding the 3D doping limit by an order of magnitude. Once formed, these self-organized surface phases are stabilized by covalent bonds in the silicon lattice. In our work, we have routinely used 2D sheet densities of 2×10^{14} B/cm^2; however, 2D doped surfaces with single-layer sheet densities as high as 3×10^{14} B/cm^2 have been demonstrated.

3.2 Superlattice-doped detectors: Modeling DUV Damage

Superlattice-doping represents a fundamentally different approach to surface doping and passivation than the conventional methods of ion implantation and diffusion. The structure of a 2D doping superlattice comprises multiple layers of delta-doped silicon grown epitaxially on a silicon surface. We have grown 2D doping superlattices with periods of up to four layers on BSI detectors, using an interlayer separation of 1 nm. Crystal quality has been verified using reflection high-energy electron diffraction during and after growth, and dopant activation has been verified using Hall measurements on MBE-grown wafers. Applied to back-illuminated detectors, the superlattice forms an electrically conductive contact layer and a potential barrier for electrons within the first few nanometers of the surface.

Figure 4 shows that there is a qualitative as well as a quantitative difference between the stability of 3D and 2D-doped surfaces. This figure was generated using six-band $k \bullet p$ calculations of the surface band structure, in which self-consistent solutions to Poisson's and Schrödinger's equations are applied to a 2D-doping superlattice with variable interface trap densities.[30] Comparing MBE grown 3D doped silicon (Figure 4a) with an MBE grown superlattice (Figure 4b), the differences in stability are obvious. Whereas 3D doped surfaces begin to degrade when the interface trap density exceeds 10^{13} cm^{-2}eV^{-1}, the 2D doping superlattice remains stable even in heavily damaged surfaces with trap densities greater than 10^{14} cm^{-2}eV^{-1}. This result is consistent with data presented in the next section, showing that superlattice doped detectors are virtually immune to DUV-induced surface damage.[9-11]

Comparing MBE passivated surfaces (Figure 4) with ion implanted surfaces (Figure 3), we find that MBE produces an electric field that is one to two orders of magnitude stronger than the fields produced by ion implantation. The higher fields produced by MBE come from the abrupt change in dopant concentration at the MBE-substrate interface, which is a reflection of the greater control over the dopant profile enabled by MBE.

3.3 Quantum exclusion in MBE-grown superlattices

Classically, the backside potential well has been modeled as a surface dead layer. In this approximation, all photogenerated charge produced within the dead layer is lost to trapping and recombination. This assumption breaks down when the surface dopant concentration is high enough that the depletion layer is only a few nanometers wide. On this length scale, quantum confinement in the backside potential well divides the conduction band into a finite number of 2D subbands. The energies of the subbands can be computed for a given detector structure and interface trap density by solving Poisson and Schrödinger equations self-consistently. One finds that at sufficiently high surface doping concentrations, there are no confined states in the backside potential well. In such cases, the backside potential well cannot trap photogenerated electrons, effectively eliminating the "dead layer." Here we can say that trapping is eliminated by quantum exclusion of electrons from the depletion layer. While achieving this condition does not preclude recombination, it does reduce the residence time of electrons near the interface, which is the best result that can be achieved. Combined with a strong enough electric field, quantum exclusion can effectively eliminate surface recombination by reducing the surface exposure of photogenerated electrons to less than a picosecond.

Figure 5 further illustrates the stability of a 2D doping superlattice compared to 3D doped surfaces, by mapping the number of confined subbands in the surface potential well as a function of the interface trap density. The white areas in these contour maps indicate regions of parameter space corresponding to the elimination of trapping by quantum exclusion. Comparison of Figures 5a and 5b shows that quantum exclusion cannot be achieved with 3D doping at interface trap densities greater than 3×10^{13} cm^{-2}eV^{-1} due to the practical limits of 3D doping, which cannot be increased arbitrarily. Precipitation and interstitial incorporation of dopants result in incomplete electrical activation and a decline in crystal quality at dopant concentrations above $\sim3\times10^{20}$ cm^{-3}. Superlattice doping can achieve quantum exclusion at trap densities greater than 10^{14} cm^{-2}eV^{-1}, simply by growing a cap layer less than 1 nm wide, which is easily achievable with MBE.

Downloaded From: http://spiedigitallibrary.org/ on 02/05/2015 Terms of Use: http://spiedl.org/terms

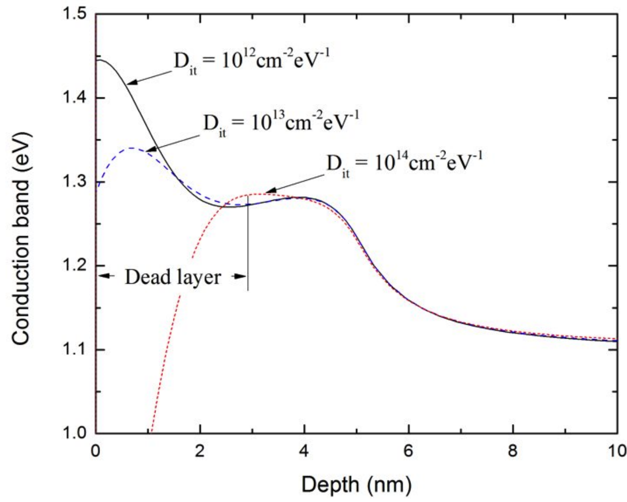

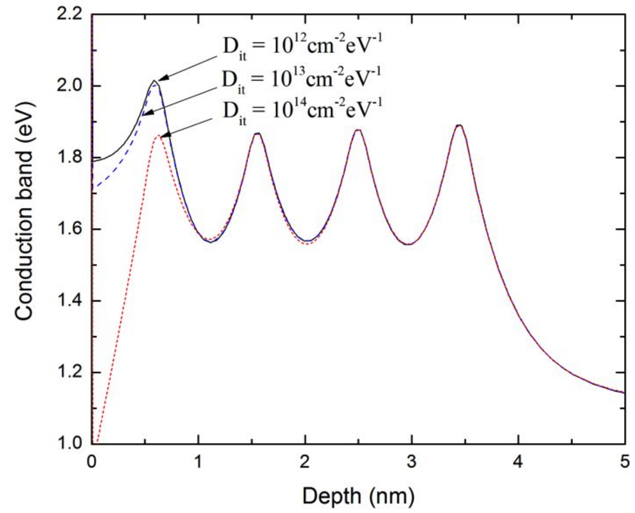

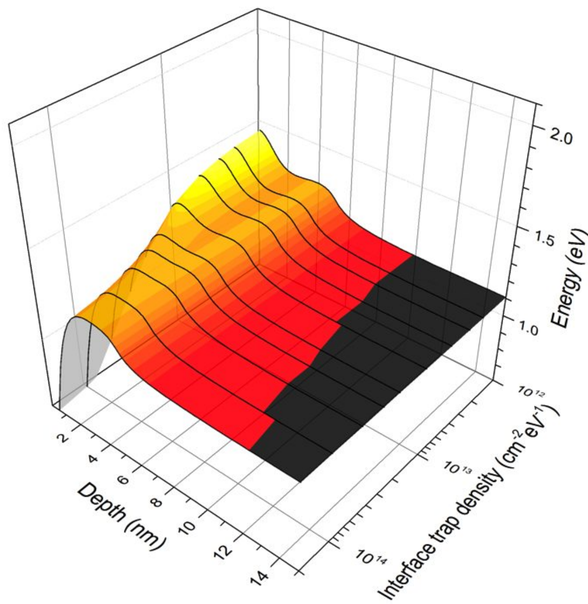

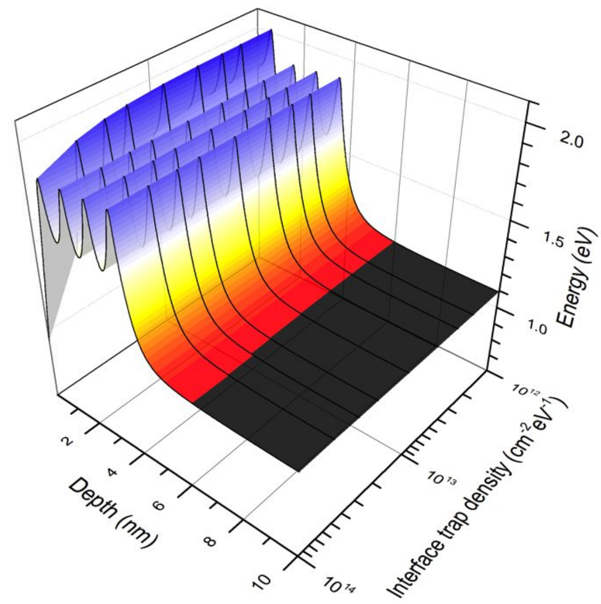

(a) MBE 3D doping $2x10^{20}cm^{-3}$

(b) MBE 2D doping superlattice

Figure 4. This figure illustrates the difference between 2D and 3D doped layers grown by molecular beam epitaxy. Figure 4a represents a uniform (3D) doped surface, comprising a 5 nm MBE layer with $2x10^{20}$ cm^{-3} boron doping, which is near the maximum that can be achieved with high quality silicon. Figure 4b represents a four-layer superlattice grown by MBE, in which four 2D-doped layers are separated by 1 nm. Several significant features are apparent in the plots. First, 3D doping creates a maximum field of 10^6 V/cm, while 2D doping creates a maximum field of 10^7 V/cm, thus exceeding the maximum field produced by ion implantation by one to two orders of magnitude. Second, the 2D doping superlattice forms a surface depletion layer with a fixed width of less than 1 nm. This depletion layer is stable against interface trap densities in excess of 10^{14} cm^{-3}, enabling the detector to remain stable even when the surface is severely damaged by irradiation by DUV lasers.

Downloaded From: http://spiedigitallibrary.org/ on 02/05/2015 Terms of Use: http://spiedl.org/terms

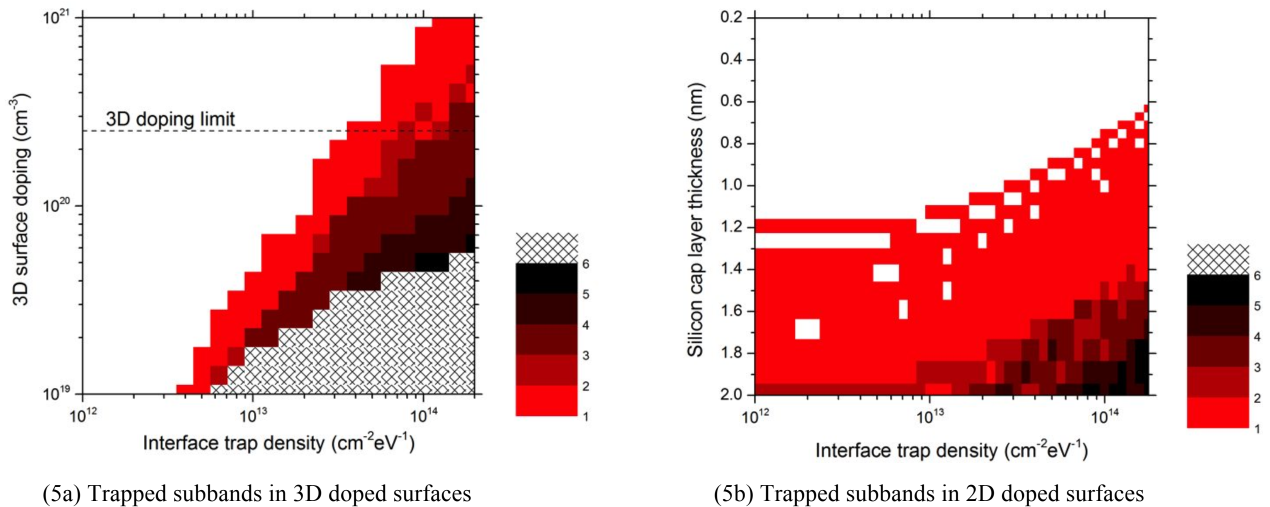

(5a) Trapped subbands in 3D doped surfaces

(5b) Trapped subbands in 2D doped surfaces

Figure 5. Contour maps presented here represent the results of thousands of surface simulations to track the relationship between doping profile, interface trap density, and the number of confined subbands. For each combination of doping and trap density, the contour maps provide a color-coded representation of the number of quantum-confined subbands in the surface depletion layer. The white regions map the parameter space in which the depletion layer is incapable of trapping electrons due to quantum exclusion. At trap densites greater than $3x10^{13}$ cm^{-2}eV^{-1}, quantum exclusion cannot be achieved by 3D doping methods. Superlattice doping enables quantum exclusion over the entire range of trap densities, simply by choosing a surface cap layer thickness of less than 1 nm, which is easily attainable by MBE. This result is consistent with DUV lifetime measurements performed on superlattice-doped, BSI CMOS imaging detectors.

4. PERFORMANCE OF SUPERLATTICE DOPED DETECTORS

4.1 Growth of 2D Doping Superlattices on BSI CMOS Detectors

Wafer-scale molecular beam epitaxy was used to grow 2D-doping superlattices on the back surface of bonded, thinned CMOS detector arrays. Detector wafers comprising 64 CMOS arrays were bonded to a silicon wafer for mechanical support and back-thinned at JPL to expose the 5 μm epilayer. JPL grew a two layer doping superlattice on the thinned detectors at full 200 mm wafer scale using a Veeco Gen 200 MBE system. Each of the layers contained a sheet of boron atoms with a surface density of $2x10^{14}$ cm^{-2}, with an interlayer spacing of 1 nm. A 2.5 nm silicon cap layer was grown on the superlattice to stabilize and protect the superlattice. Devices used in 263 nm experiments included a 28 nm Al_2O_3 antireflection (AR) coating grown using an Oxford OpAL ALD system. Devices used in 193 nm experiments were not AR-coated.

4.2 Measurements of DUV-induced Interface Trap Densities

As described above, DUV-induced surface damage causes severe degradation of BSI detectors. Band structure calculations presented in the last section indicate that superlattice-doped detectors should be uniquely insensitive to DUV damage. One important question concerns the magnitude of surface damage induced by DUV exposure. Knowledge of this parameter informs the design 2D doping superlattice and the limits of DUV stability.

By the early 1960's, measurements of atomically clean silicon had confirmed that the surface state density corresponds to the number of "dangling" bonds on the exposed surface.[32] This sets an approximate upper limit of $6.8x10^{14}$ cm^{-2} for the interface trap density on a bare (100) silicon surface. However, atomically clean surfaces are not stable, and the interface trap density is significantly reduced upon exposure to air and the formation of a native oxide. Silicon surfaces passivated with high quality thermal oxides exhibit significantly lower trap densities. By combining thermal oxidation with hydrogen passivation, interface trap densities below 10^{10} cm^{-2}eV^{-1} can be routinely achieved in MOS devices. In MOS devices, trap densities greater than 10^{12} cm^{-2}eV^{-1} are considered extreme. Damage from DUV exposure is significantly more extreme. Interface trap densities in the range of 10^{14} cm^{-2}eV^{-1} have been observed following exposure to vacuum ultraviolet radiation.[19]

Downloaded From: http://spiedigitallibrary.org/ on 02/05/2015 Terms of Use: http://spiedl.org/terms

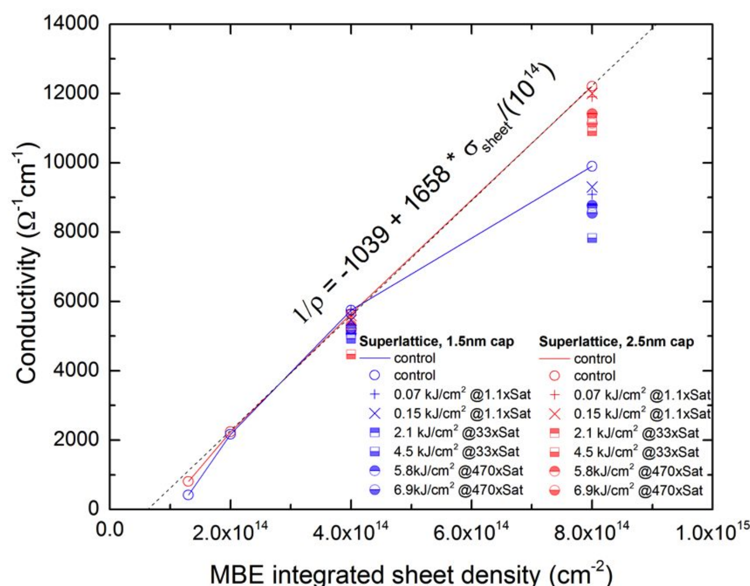

Figure 6. Measurements of the conductivities of superlattice doped surfaces before and after exposure to deep ultraviolet lasers demonstrate severe degradation of the surface conductivity. Based on these data, it is estimated that DUV damage induces interface charge densities in the range of 10^{14} cm^{-2} in superlattice doped detectors (see text).

In order to quantify the DUV-induced surface damage created under conditions relevant to superlattice-doped detectors, we used an indirect method based on surface conductivity measurements. Because interface-trapped charge partially compensates surface doping, the conductivity of a doped surface is negatively correlated with interface trap density. The DUV exposure levels used in these experiments were designed to be comparable to DUV lifetime tests to be performed later on superlattice-doped devices. Figure 6 shows a linear fit of conductivity vs. superlattice-doping sheet density in undamaged surfaces. Note that the x-intercept is not zero, but rather ~$6x10^{13}$ cm^{-2}, which suggests that the native oxide that forms on superlattice-doped surfaces already exhibits a high density of trapped charge prior to DUV exposure. Analysis of the conductivity of DUV-damaged surfaces indicates that the density of interface-trapped charge increases by as much as 10^{14} cm^{-2}. We therefore conclude that DUV-damaged surfaces can exhibit interface charge densities approaching $2x10^{14}$ cm^{-2}. This result is comparable to measurements of extreme levels of damage to Si-SiO_2 interfaces caused by exposure to vacuum ultraviolet radiation.[19]

4.3 DUV Lifetime of Superlattice-doped Detectors

Superlattice-doped detectors were integrated into Alacron cameras and subjected to lifetime tests at Applied Materials using 263 nm pulsed, solid state and 193 nm pulsed excimer lasers. The sensor was illuminated with a 193 nm excimer pulsed DUV laser that emitted collimated 10 ns pulses at 1000 Hz, at a duty factor (DF) of 67% (2 sec ON, 1 sec OFF). A set of 2 optical diffusers in tandem comprised the beam-shaping optics that provided a Flat-Field (FF) illumination of the surface of the sensor at an energy density of 80 nJ/cm^2, which corresponds to the saturation exposure of this detector. A slit of controlled size and position in front of the camera, served to illuminate a distinct area inside the FOV of the sensor while the rest of the sensor was covered for reference (Figure 5). When the response of the sensor was monitored, the slit was moved out of the line-of-sight and the sensor was exposed to a FF illumination. Following a short monitoring session, the slit replaced the FF in front of the sensor (with a repetition of ~1 pixel) for further accumulation of DUV exposure pulses. The sensor received ~60 MP of 1 saturation exposure per each 24 h, and its degradation was monitored on a daily basis.

Cameras' electronic noises are subtracted to accurately measure the physical stability of the photo response mechanism. Figures 7 and 8 show an analysis of a 100 consecutive images comprising 2.1 billion laser pulses at 193 nm. Following >2 billion laser pulses at full saturation, there is no evidence of any degradation of the illuminated area (within 1%) (Figure 8). Current estimates are that actual lifetime exceeds 10 B laser pulses. Superlattice doping technology was also

Downloaded From: http://spiedigitallibrary.org/ on 02/05/2015 Terms of Use: http://spiedl.org/terms

verified to meet inspection requirements by measurement of the internal QE to be ~100% (excluding quantum yield), with no blooming and no image memory observed at 1000 fps.

A similar test setup with a pulsed 263 nm laser on an AR coated sensor, at up to x257 camera saturations, showed no measurable degradation following an accumulated illumination dose of 3100 J/cm^2. No blooming and no image memory were present even at the high saturation levels. The sensor also demonstrated a high modulation transfer function (MTF) (Figure 9).

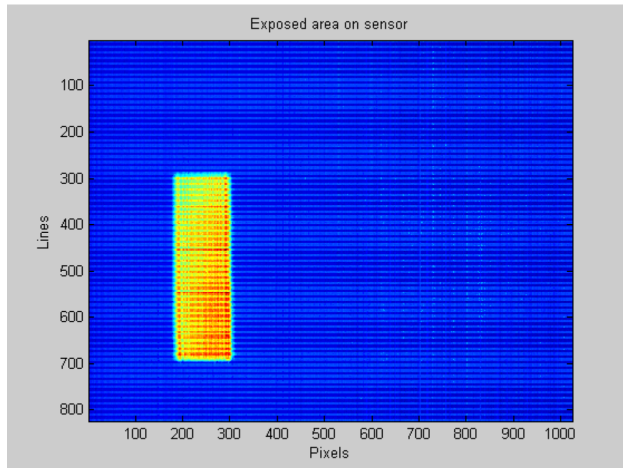

Figure 7. Exposure slit position on sensor

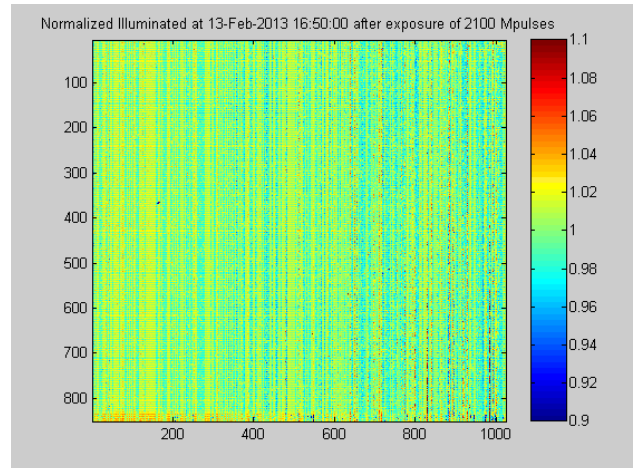

Figure 8. Normalized spatial response of superlattice doped detector following 2.1 B pulses at 193 nm. No degradation in quantum efficiency or dark current is observed at 1% precision.

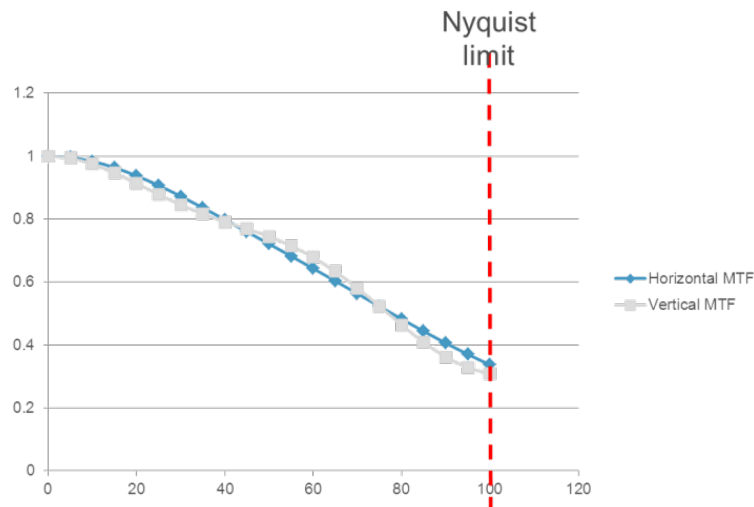

Figure 9. Horizontal and vertical MTF of the sensor

5. ATOMIC LAYER DEPOSITION OF MULTILAYER COATINGS

5.1 Solar blind coatings

It is possible to integrate visible and solar rejection filters directly onto a silicon sensor for UV detection applications where it is desirable to reject response to longer wavelength light. Metal dielectric filters (MDF), also known as Fabry-Perot filters or photonic bandgaps have a long history of use as bandpass filters in the UV.[33] In these structures matched parallel reflecting plates are separated by a transparent spacer layer in order to destructively phase-match the reflection off of one metal layer at a particular wavelength and therefore maximize transmission through the structure. Out of band

Downloaded From: http://spiedigitallibrary.org/ on 02/05/2015 Terms of Use: http://spiedl.org/terms

light is not subjected to the same interference and is therefore rejected by the high natural reflectance of the stack. By extending MDFs for use directly on a silicon photodetector it is possible to obtain superior transmission/rejection performance when compared to similar structures fabricated on transparent substrates as stand-alone filter elements.[13]

For applications where large out-of-band rejection is not required, simple three layer dielectric-aluminum-dielectric structures are capable of a peak transmittance of greater than 90% over most of the UV range from 100 to 300 nm, a significance improvement over the performance of simple dielectric based AR coatings in this spectral range. Increasing the number of the cavities can result in much larger rejection ratios by trading off some amount of peak transmission. For example, calculated models of a seven layer aluminum-based MDF on silicon can achieve five orders of blocking for wavelengths greater than 300 nm while still providing a peak transmission greater than 50% for target wavelengths near 200 nm.

Test MDF structures were fabricated on silicon photodiodes for an application designed to maximize transmission at 220 nm while rejecting incident light at 310 nm. Three layer (one cavity) and five layer (two cavities) MDFs were designed to have modeled peak transmissions of 75% and 60%, and rejection ratios greater than 10:1 and 500:1, respectively. Al_2O_3 deposited by ALD was used as the dielectric spacer because it is transparent in this wavelength range and also has an inherent chemical stability with the metallic aluminum reflector layer. The aluminum layer was evaporated by electron beam with thickness monitored by quartz crystal microbalance. No particular precaution was taken to prevent ambient exposure of the evaporated aluminum films prior to ALD, samples were transferred ex-situ. Co-deposited witness samples were characterized by spectroscopic ellipsometry and reflectivity measurements and correlate well with calculated predictions and with measurements of photodiode QE.

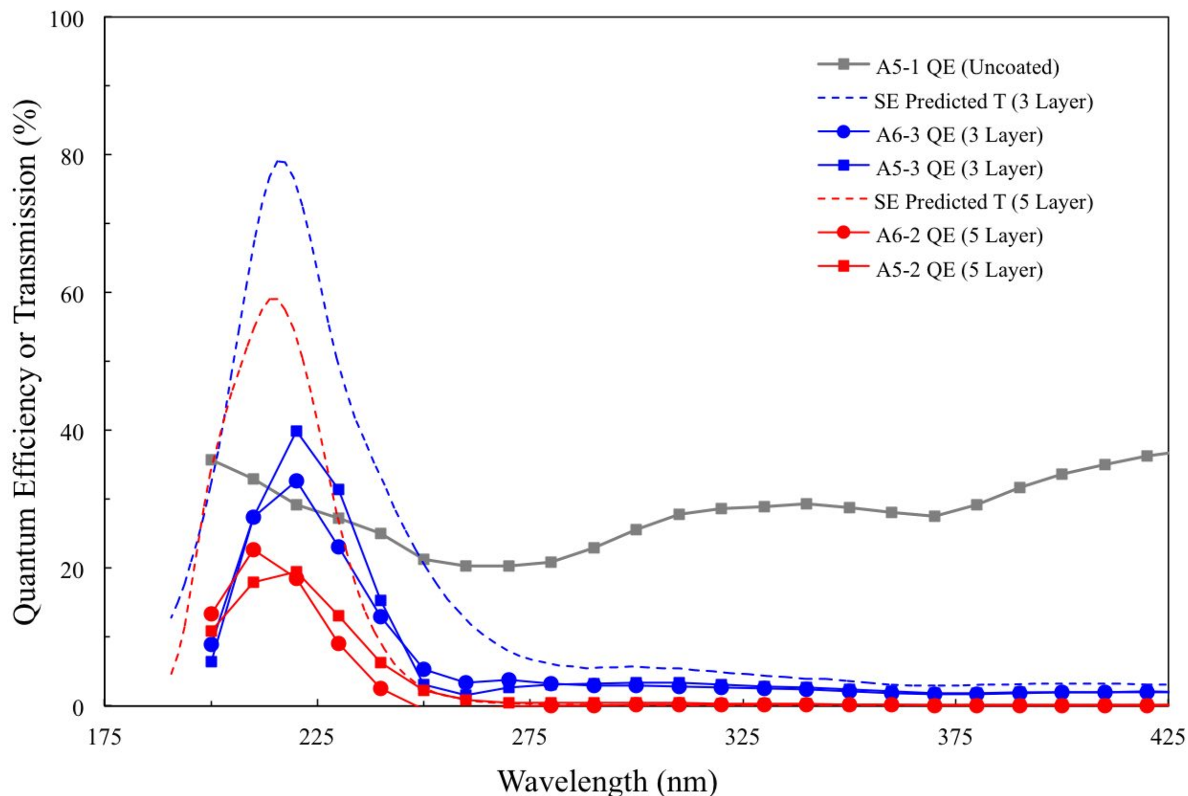

Figure 10. Comparison of measured QE and model results for superlattice doped avalanche photodiodes coated with metal dielectric filters. Experimental results provide a proof-of-concept demonstration of integrated, solar-blind filters on superlattice doped detectors. Discrepancies between data and models are attributed to residual contamination from dicing and die-level AR coating of the prototype detectors. The next set of detectors will eliminate this source of contamination by using wafer scale MBE and wafer scale ALD in immediate succession.

Downloaded From: http://spiedigitallibrary.org/ on 02/05/2015 Terms of Use: http://spiedl.org/terms

6. ACKNOWLEDGEMENTS

The research described in this paper was carried out at the Jet Propulsion Laboratory, California Institute of Technology, under a contract with the National Aeronautics and Space Administration. The authors would like to thank Suzannah Riccardi and Richard Myers of Radiation Monitoring Devices for quantum efficiency measurements on superlattice-doped avalanche photodiodes.

REFERENCES

[1] Michael E. Hoenk, Paula J. Grunthaner, Frank J. Grunthaner, R. W. Terhune, Masoud Fattahi, and Hsin-Fu Tseng, "Growth of a delta-doped silicon layer by molecular beam epitaxy on a charge-coupled device for reflection-limited ultraviolet quantum efficiency," *Appl. Phys. Lett.* **61**, 1084 (1992).

[2] S. Nikzad, M. E. Hoenk, P. J. Grunthaner, R. W. Terhune, F. J. Grunthaner, R. Winzenread, M. Fattahi, H-F. Tseng, M. Lesser, "Delta-doped CCDs: High QE with long-term stability at UV and visible wavelengths," *Instrumentation for Astronomy VIII*, SPIE Proc. **2198**: 907 (1994).

[3] Shouleh Nikzad; Todd J. Jones; S. T. Elliott; Thomas J. Cunningham; Peter W. Deelman; Arthur B. C. Walker; Hakeem M. Oluseyi, "Ultrastable and uniform EUV and UV detectors," Proc. SPIE 4139, Instrumentation for UV/EUV Astronomy and Solar Missions, 18 December (2000).

[4] Michael E. Hoenk, T. J. Jones, M. R. Dickie, H.F. Greer, T. J. Cunningham, E. Blazejewski, S. Nikzad, "Delta-doped back-illuminated CMOS imaging arrays: progress and prospects," Proc. SPIE 7419B-34, *Infrared Detector Devices and Photoelectronic Imagers IV*, 2009.

[5] S. Nikzad, M. E. Hoenk, F. Greer, B. Jacquot, S. Monacos, T. Jones, J. Blacksberg, E. Hamden, D. Schiminovich, C. Martin, P. Morrissey, "Delta doped Electron Multiplied CCD with Absolute Quantum Efficiency over 50% in the near to far Ultraviolet Range for Single Photon Counting Applications," *Applied Optics*, Vol. 51, Issue 3, pp. 365-369 (2012).

[6] F. Greer, E. Hamden, B. C. Jacquot, M. E. Hoenk, , T. Jones, M. Dickie, S. P. Monacos, S. Nikzad, "Atomically Precise Surface Engineering of Silicon CCDs for Enhanced UV Quantum Efficiency", *Journal of Vacuum Science and Technology A*, 01A103-1 (2013).

[7] April D. Jewell, John Hennessy, Michael E. Hoenk, Shouleh Nikzad, "Wide band antireflection coatings deposited by atomic layer deposition," Proc. SPIE 8820, Nanoepitaxy: Materials and Devices V, (2013).

[8] S. Nikzad, M. E. Hoenk, A. G. Carver, T.J. Jones, F. Greer, E. Hamden, and T. Goodsall, "High Throughput, High Yield Fabrication of High Quantum Efficiency Back- illuminated Photon Counting, Far UV, UV, and Visible Detector Arrays," Proceedings of the 2013 International Image Sensor Workshop, Snowbird, Utah, 13 June 2013.

[9] Hoenk, M. E., "Surface Passivation by Quantum Exclusion Using Multiple Layers," U.S. Patent Number 8,395,243, issued 3/12/2013.

[10] Hoenk, M. E.; Carver, A. G.; Jones, T. J.; Dickie, M.; Cheng, P.; Greer, F.; Nikzad, S.; Sgro, J.; Tsur, S.; "The DUV Stability of Superlattice-doped CMOS Detector Arrays," Proceedings of the 2013 International Image Sensor Workshop, Snowbird, UT, June 12-16, 2013.

[11] Hoenk, M.E., A.G. Carver, T.J. Jones, M. Dickie, S. Nikzad, J. Sgro, S. Tsur, "Superlattice-doped Imaging Detectors: Structure, Physics, and Performance," Proceedings of the Scientific Detectors Workshop, Florence, Italy, October 7-11, 2013.

[12] F. Greer, S. Nikzad, "Methods to Fabricate and Improve Stand-Alone and Integrated Filters," U.S. Patent Pending.

[13] J. Hennessy, A.D. Jewell, M.E. Hoenk, S. Nikzad. "Silicon Integrated Metal Dielectric Filters for the Ultraviolet," to be submitted (2014).

[14] Li, F; Nixon, O; Nathan, A; "CCD Detection of 157 nm photons," Proc. IEEE Workshop on Charge-Coupled Devices and Advanced Image Sensors, Elmau, Germany, 2003.

[15] Li, FM & Nathan, A, *CCD image sensors in deep-ultraviolet: degradation behavior and damage mechanisms*, Springer, Berlin, 2005.

[16] Arp, U., Shaw, P.S., Gupta, R. and Lykke, K.R., "Damage to solid-state photodiodes by vacuum ultraviolet radiation," *J. Electron Spectroscopy and Related Phenomena*, **144-147**: 1039-1042, 2005.

[17] Defise, J.M.; Moses, J.D.; Clettec, F; EIT Consortium, "In-orbit performances of the EIT instrument on-board SOHO and intercalibration with the EIT Calroc Sounding rocket program," *Proc. SPIE 3442*, Missions to the Sun II, 126 (November 2, 1998).

Downloaded From: http://spiedigitallibrary.org/ on 02/05/2015 Terms of Use: http://spiedl.org/terms

[18] William T. Thompson, "UV detectors aboard SOHO," Proc. SPIE 3764, Ultraviolet and X-Ray Detection, Spectroscopy, and Polarimetry III, 196, November 1999.
[19] Afanas'ev, V.V., de Nijs, J. M. M., and Balk, P., "Degradation of the thermal oxide of the Si/SiO_2/Al system due to vacuum ultraviolet radiation," *J. Appl. Phys.*, **78**(11): 6481-6490, 1995.
[20] Raj Korde and Jon Geist, "Quantum efficiency stability of silicon photodiodes," Applied Optics, 26(24): 5284-5290, 1987.
[21] Raj Korde, James S. Cable, and L. Randall Canfield, "One Gigarad Passivating Nitrided Oxides for 100% Internal Quantum Efficiency Silicon Photodiodes," *IEEE Transactions on Nuclear Science*, **40**(6): 1655-1659, 1993.
[22] R. Korde, C. Prince, D. Cunningham, R. E. Vest, and E. Gullikson, "Present status of radiometric quality silicon photodiodes," *Metrologia*, **40**: S145-149, 2003.
[23] Michael Lesser and Venkatraman Iyer, "Enhancing back illuminated performance of astronomical CCDs," Proc. SPIE 3355, Conference on Optical Astronomical Instrumentation, pp. 446-456, March 1998.
[24] James Janesick, Tom Elliott, Taher Daud, Jim McCarthy, Morley Blouke, "Backside charging of the CCD," Proc. SPIE 570, Solid State Imaging Arrays, 46-79, 1985.
[25] James Janesick, Tom Elliott, George Fraschetti, Stewart Collins, Morley Blouke, et al., "Charge-Coupled Device Pinning Technologies," Proc. SPIE 1071, Optical Sensors and Electronic Photography, 153, May 23, 1989.
[26] R.A. Stern, R.C. Catura, R. Kimble, A.F. Davidsen, M. Winzenread, M.M. Blouke, R. Hayes, D.M. Walton, J.L. Culhane, "Ultraviolet and extreme ultraviolet response of charge-coupled device detectors," Optical Engineering, 26(9): 875-883, 1987.
[27] Paul Jerram, David Burt, Neil Guyatt, Vincent Hibon, Joel Vaillant, Yann Henrion, "Back-thinned CMOS Sensor Optimisation," Proc. SPIE 7598, Optical Components and Materials VII, 759813, 2010.
[28] N.R. Collins, N. Boehm, G. Delo, R. D. Foltz, R. J. Hill, E. Kan, R. A. Kimble, E. Malumuth, R. Rosenberry, A. Waczynski, Y. Wen, S. Baggett, H. Bushouse, S. Deustua, J. Kim-Quijano, J. MacKenty, A. Martel, E. Sabbi, "Wide Field Camera 3 CCD Quantum Efficiency Hysteresis: Characterization and Mitigation," Proc. SPIE 7439, Astronomical and Space Optical Systems, 74390B, 2009.
[29] Deiries S., Downing M., Baade D., 2009, "CCD UV QE Improvement by Gas and Thermal Treatment," ESO Garching, 12 - 16 October 2009.
[30] Birner, S.; Hackenbuchner, S.; Sabathil, M.; Zandler, G.; Majewski, J.A.; Andlauer, T.; Zibold, T.; Morschl, R.; Trellakis, A.; & Vogl, P., "Modeling of Semiconductor Nanostructures with nextnano3," *Acta Physica Polonica A*,110(2): 111-124, 2006.
[31] Michael E. Hoenk, Paula J. Grunthaner, Frank J. Grunthaner, R. W. Terhune, and Masoud Fattahi, "Epitaxial growth of p+ silicon on a backside-thinned CCD for enhanced UV response," Proc. SPIE 1656, 488, 1992.
[32] E. H. Nicollian, "Surface passivation of semiconductors," Journal of Vacuum Science and Technology, 8(5): S39-S49, 1971.
[33] B. Bates and D. J. Bradley, "Interference Filters for the Far Ultraviolet (1700 Å to 2400 Å)," *Applied Optics*, 5(6): 971-975, 1966.

Downloaded From: http://spiedigitallibrary.org/ on 02/05/2015 Terms of Use: http://spiedl.org/terms